



Ingestion of GIM-derived TEC data for updating IRI-2016 driven by effective IG indices over the European region

Lei Liu^{1,2} · Yibin Yao^{1,3,4} · Shasha Zou² · Jian Kong⁵ · Lulu Shan¹ · Changzhi Zhai¹ · Cunjie Zhao¹ · Youkun Wang^{1,6}

Received: 25 January 2019 / Accepted: 16 August 2019 / Published online: 28 August 2019
© Springer-Verlag GmbH Germany, part of Springer Nature 2019

Abstract

In order to adapt the International Reference Ionosphere (IRI) model from ionospheric climatological model to near real-time weather predictions, total electron content (TEC) data from Global Ionosphere Maps are ingested into the IRI-2016 model through retrieving the optimal ionospheric index (IG) over Europe on an hourly basis. When the retrieved hourly effective IG indices are used to drive the IRI-2016 model, the resulting ionospheric parameters are externally evaluated with respect to multiple sources, including the COSMIC/ionosonde electron density (Ne) profiles, ionosonde F2 layer critical frequency (foF2), and individual GNSS-derived TEC for both quiet and storm conditions. Results show that: (1) The updated IG indices for different latitudinal zones tend to follow a similar trend under quiet conditions, but vary much more significantly during storm days. (2) The retrieved Ne profiles from the updated IRI-2016 agree better with those from the COSMIC Ne profiles, especially for the F2 layer maximum electron density (NmF2) values. Furthermore, the updated IRI-2016 Ne profiles show improved agreement with ionosonde measurements under quiet conditions, particularly for the bottom-side Ne profiles and NmF2 as well as for the storm-time Ne profiles. (3) Comparing the IRI-updated TEC with the GNSS-derived TEC, IRI-updated TEC improved approximately 19% for both quiet and storm days, and the nighttime TEC improvement is better than that during daytime. When compared to the ionosonde foF2 measurements, the daytime IRI-updated foF2 improvement during quiet time is better than that during storm condition, while the performance for nighttime foF2 drops during quiet time. Discussions about possible reasons for the nighttime foF2 degradation are included.

Keywords GIM-derived TEC · IRI-2016 · IG index · Ingestion method

1 Introduction

The ionosphere is the ionized part of the earth's upper atmosphere, and it is arguably the most important region in terms of space weather impact. Therefore, it is of significant practical importance to model the spatial and temporal structures of the ionosphere. The IRI model is an international project sponsored by the Committee on Space Research (COSPAR) and the International Union of Radio Science (URSI) with the goal of developing and improving an international standard for ionospheric parameters (Bilitza et al. 2011, 2014, 2017). The IRI model, as the most widely used empirical climatological model of the ionosphere, provides various ionospheric parameters, such as electron density (Ne) profiles, TEC, ion and electron temperatures, and critical frequencies in the altitude range of 60–2000 km, and without doubt, aids in the study of the complex structures and dynamics of the ionosphere. Generally, the IRI model outputs depend on the solar (F10.7D, F10.7_81, SSN, R12) and ionospheric (IG,

✉ Yibin Yao
ybyao@whu.edu.cn

¹ School of Geodesy and Geomatics, Wuhan University, Wuhan, China

² Department of Climate and Space Sciences and Engineering, University of Michigan, Ann Arbor, MI, USA

³ Key Laboratory of Geospace Environment and Geodesy, Ministry of Education, Wuhan University, Wuhan, China

⁴ Collaborative Innovation Center for Geospatial Technology, Wuhan, China

⁵ Chinese Antarctic Center of Surveying and Mapping, Wuhan University, Wuhan, China

⁶ Kunming Surveying and Mapping Institute, Kunming, China

IG12) indices as input to the model. The solar indices reflect the ionosphere variations due to changing solar radiation, while the ionospheric indices, based on actual measurements (e.g., ionosonde, ISR and GPS data), can capture some additional ionospheric effects that may also vary with solar activity (Bilitza et al. 1997; Chen et al. 2011; Brown et al. 2017; Gulyaeva et al. 2018).

Similar to many ionospheric empirical climatological models, IRI is not able to accurately describe ionospheric dynamics, especially under storm conditions, though a storm option is included in IRI model (Araujo-Pradere E et al. 2002; Bilitza et al. 2014). Thus, many attempts and approaches have been proposed to upgrade the IRI model with more ionospheric measurements and sophisticated techniques becoming available. For example, the ionospheric global (IG) index and its 12-month running mean IG12 are important ionospheric activity indices to drive the IRI model, and Liu et al. (1983) developed the IG index by adjusting the CCIR foF2 model to fit the monthly noontime critical frequency foF2 values observed at several ionosonde stations. As a result, it successfully reflected ionosphere variations that are not described by the solar indices. Bilitza et al. (1997) used foF2 measurements from more than 70 ionosondes worldwide to calculate the IG12 index. They found that zonally averaged updated IG12 indices could improve the IRI estimates for the GEOSAT time period (1986–1989) by a few percent, which thus highlights the importance of IG12 spatial characterization. Recently, Brown et al. (2017) introduced a monthly hemispheric IG^{NS} index (similar to the construction of the IG given by Liu et al. (1983), but not 12-month smoothed IG index) based on worldwide ionosonde foF2 measurements, and the results show that the inclusion of the new monthly IG^{NS} index improved outputs of the foF2 solar cycle variations. In addition, Pignalberi et al. (2018) adjusted effective 12-month running mean of the sunspot number (R12) and IG12 indices to update the IRI model through assimilating ionosonde data over Europe, and the proposed method turned out to be very effective with significant improvements of the foF2 and hmF2 parameters, especially under highly disturbed conditions.

In addition to the aforementioned IRI assimilation methodology based on the ionosonde data, GNSS-derived TEC data have also been found to be helpful and promising in improving the IRI model results. For example, Komjathy and Langley (1996) investigated the use of TEC estimates from dual-frequency GPS receiver observations to update the IRI-95 model on an hourly basis and found that the original model performance was improved overall by 32.5%. A similar approach was also pursued by Hernandez-Pajares et al. (2002), who used 2-hour GIM-derived TECs, with a spatial resolution of 2.5° in latitude and 5° in longitude, to improve the IRI TEC capability. Finally, they performed a local fit of the IRI model by tuning the sunspot number

(SSN) from GPS-based slant TEC (STEC) measurements, and IRI predictions agree well with the GPS estimations for middle latitudes. Okoh et al. (2013) calibrated the IRI 2012 model using GPS-derived TEC, and the results show that RMS decreases from 22.81 to 1.80 TECu when the IRI model is corrected using GPS VTEC from the Nsukka station. Migoya-Oru e et al. (2015) ingested GIM-derived TEC into the IRI 2012, aiming to obtain grids of effective input parameter values that allow for the minimization of the difference between the experimental and modeled TEC. It is found that the retrieved foF2 presentation was enhanced compared to worldwide ionosondes, especially for high solar activities. Habarulema and Ssessanga (2017) reported the modification of the IRI-2012 model with adjusted R12 and IG12 indices by minimizing error differences between IRI TEC and GNSS TEC over the African sector and achieved its direct validation in terms of IRI parameters with radio occultation and ionosonde data for both quiet and disturbed periods. Recently, Aa et al. (2018) ingested the Madrigal TEC data into the NeQuick-2 model through deriving an effective ionization parameter (A_z), and the results show that a general accuracy improvement of 30–50% can be achieved after data ingestion.

Overall, many assimilation/ingestion procedures have been used to update the IRI model, while most of them have limited success in reflecting the short-term or local dynamical changes of the ionosphere, particularly under disturbed conditions, such as geomagnetic storms. On the other hand, the latest version of the IRI model (IRI-2016) aims to make progress from predicting the climatology of ionosphere to describing the real-time weather conditions in the ionosphere (Bilitza et al. 2017). In this work, we try to generate hourly IG indices in each latitudinal zone by ingesting GIM-derived TEC into the IRI-2016 model, and then the resulting IG indices are regarded as the effective drivers of the IRI-2016 model to yield short-term ionospheric parameters (such as electron density profiles, TEC, foF2 or NmF2). These reproduced ionospheric parameters are also externally evaluated COSMIC/ionosonde electron density profiles and ionosonde foF2 values, as well as GNSS-derived TEC data.

2 Data and methodology

The IRI model provides climatological behavior of TEC integrated from 60 to an altitude of 2000 km. Similarly, the International GNSS Service (IGS) center provides GIM TEC products, but up to the GNSS satellite orbit (20,200 km). It is necessary to develop IG indices by minimizing the difference between the IRI-2016 TEC and GIM-derived TEC, and then the new IG index is used as the effective ionosphere index to drive the IRI-2016 model. It should be noted that the integration upper altitudes for the IRI-generated TEC

(2000 km) and the GIM-derived TEC (20,200 km) are different, which means the GIM-derived TEC contains the plasmaspheric contribution. Many studies reported that the plasmaspheric contribution to TEC can potentially be up to 20% and 50% for daytime and nighttime, respectively (Yizengaw et al. 2008; Klimenko et al. 2015; Liu et al. 2018), thus causing the TEC mismatch between IRI and GNSS calculations that can degrade the IRI results regardless of the ingestion method. In our procedure, the plasmaspheric electron content (PEC) from 2000 to 20,200 km contained in the GIM-derived or GNSS-based TEC from individual stations is derived from the NeQuick-2 model, which is the latest version of the NeQuick three-dimensional and time-dependent ionospheric electron density model (Nava et al. 2008). Then the PEC is subtracted from the GIM-derived or GNSS-based TEC. Finally, we generate hourly IG indices to update the IRI-2016 model by ingesting GIM-derived TEC. In the model modification process, the FORTRAN source code of the IRI-2016 was used, and more details about the IRI model can be found on <http://irimodel.org>.

2.1 Description of data

The chosen time period from DOY074 to DOY077 (March 15 to 18, 2015) contains both quiet days and an intense geomagnetic storm, the so-called St. Patrick geomagnetic storm (Cherniak et al. 2015; Astafyeva et al. 2015; Yao et al. 2016). The considered time period was characterized initially by a magnetically quiet period despite a few substorms, as shown by the Dst and AE parameters in the top panel of Fig. 1, lasting until the storm sudden commencement (SSC)

registered at 04:45 UT on March 17 (DOY076). Afterward, the development of the storm can be divided into three typical stages: the initial phase (04:45–07:30 UT), the main phase (07:30–22:45 UT), and the recovery phase (after 22:45 UT).

Based on GNSS dual-frequency code and phase measurements from globally distributed IGS tracking stations, it is possible to obtain GIM TEC products. Currently, seven Ionospheric Associate Analysis Centers (IAACs) are the main contributors to the GIM-derived TEC maps, which have a spatial resolution of 2.5° in latitude and 5° in longitude. In this study, hourly GIM-derived TEC obtained from the CODE analysis center over the European sector (40–60° in latitude, 0–20° in longitude) is ingested into the IRI-2016 model, and then an evaluation is performed to test whether the IRI-2016 output parameters will be improved. Additionally, ionosonde data (<ftp.ngdc.noaa.gov/ionosonde/data/>, see

Table 1 Ionosonde stations from which data are used for validating the updated IRI-2016 electron density and foF2 parameters

Ionosonde stations	URSI ID	Geographical Lat (°)	Geographical Lon (°)	Ionosonde type
Juliusruh	JR055	54.6	13.4	DPS-4D
Chilton	RL052	51.5	-0.6	DPS-1
Dourbes	DB049	50.1	4.6	DPS-4D
Pruhonic	PQ052	50	14.6	DPS-4D
Rome	RO041	41.8	12.5	AIS-INGV
Roquetes	EB040	40.8	0.5	DPS-4D
San Vito	VT139	40.6	17.8	DPS-4D

Fig. 1 Geomagnetic indices (Dst and AE, top panel) and solar activity indices (sunspot number and F10.7, bottom panel) for the studied period. The geomagnetic/solar activity indices data are obtained from the NASA Goddard Space Flight Center (<https://spdf.gsfc.nasa.gov/index.html>)

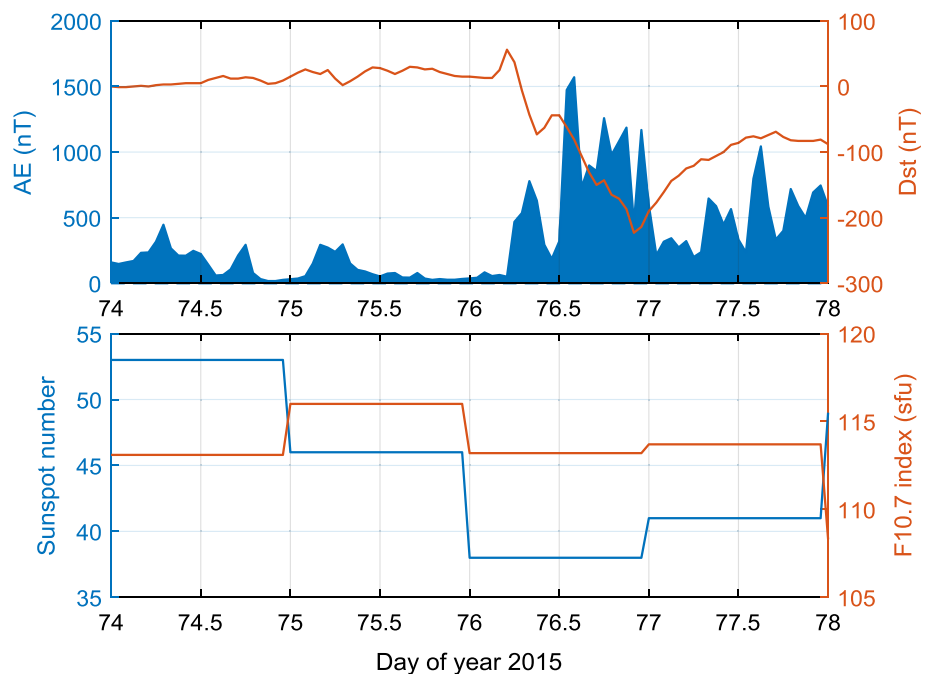


Table 2 GNSS receivers from EPN used for validating the updated IRI-2016 TEC parameter

Station code	Geographical Lat (°)	Geographical Lon (°)
STAS	59.0	5.6
JON6	57.7	14.1
HOBUB	53.1	10.5
SHOE	51.6	0.8
SMNE	48.8	2.4
CAKO	46.4	16.4
ELBA	42.8	10.1
BELL	41.6	1.4
MATG	40.6	16.7

Table 1) and GNSS data (<http://epncb.oma.be/>, see Table 2), as well as available COSMIC data (<http://cdaac-www.cosmic.ucar.edu/cdaac/>), are compared with the IRI-2016 model outputs during the selected period.

2.2 Solar and ionospheric indices for IRI model input

The IRI output parameters are usually driven by several solar and ionospheric indices. One of the most widely used solar flux indices required for IRI is F10.7, which corresponds to the integrated flux generated by the Sun at a wavelength of 10.7 cm at the earth’s orbit (Tapping 2013). The F10.7 index can be entered as a daily mean (F10.7D) value, a running mean of 81 days (F10.7_81) or a running mean of 12 months (F10.7_12). Similarly, the SSN or its 12-month running mean (R12) is also a popular solar index, which is used in both the Community Coordinated Modeling Center (CCMC) and the International Union of Radio Science (URSI) models encapsulated in the IRI for hmF2, foF1, and the bottom-side thickness parameter B0, as well as for the electron density at the D-region inflection point (Bilitza et al. 2017; Gulyaeva et al. 2018). The IG index is calculated from linear regression equations based on the CCIR model using monthly medians of the noontime foF2 at selected ionosonde stations, and the corresponding IG12 is used in CCIR and URSI to model foF2. It should be noted that all the solar indices (F10.7D, F10.7_81; SSN, R12) and the ionospheric index (IG) are required in the IRI model. An IRI user can obtain these mentioned indices from the internal apf107.dat and ig_rz.dat files or enter his/her own values for them.

In this study, the default solar indices from the apf107.dat files are used, and then we try to find the optimum value of the IG index used in IRI by minimizing the difference between the IRI-2016 TEC and the GIM-derived TEC over Europe. Furthermore, the NeQuick model is used as the topside option, and the CCIR model is considered as the Ne F-peak option in

the IRI-2016 model. Additionally, other optional parameters for the IRI-2016 model are set to default values. As a result, the updated IG index is used as a driver of the IRI-2016 model to retrieve the Ne profiles, TEC, and foF2 parameters.

2.3 IRI-2016 ingestion technique with GIM-derived TEC

On a regional scale, the research area focused in this study (40–60°N, 0–20°E over Europe) is divided into four latitudinal zones with 5° width in latitude (see Fig. 2), namely, zone₁ (60°–55°), zone₂ (55°–50°), zone₃ (50°–45°), zone₄ (45°–40°).

The regional electron content (REC) in each latitudinal zone is defined as a total number of electrons from 60 km to the GNSS satellite altitude, and it is calculated by the summation of the vertical TEC values TEC_j multiplied by the cell’s area S_j over all TEC cells in each latitudinal zone (Afraimovich et al. 2008). In our case, the mean REC \overline{REC}_k in latitudinal zone zone_k (k = 1, 2, 3, 4) for one given time is defined as follows,

$$\begin{cases} \overline{REC}_k = \frac{REC_k}{\sum_{j=1}^8 S_j}, j = 1, 2, 3, \dots, 8 \\ REC_k = \sum_{j=1}^8 TEC_j S_j \\ S_j \approx R^2 \Delta\varphi [\sin \theta_j - \sin(\theta_j + \Delta\theta)] \end{cases} \quad (1)$$

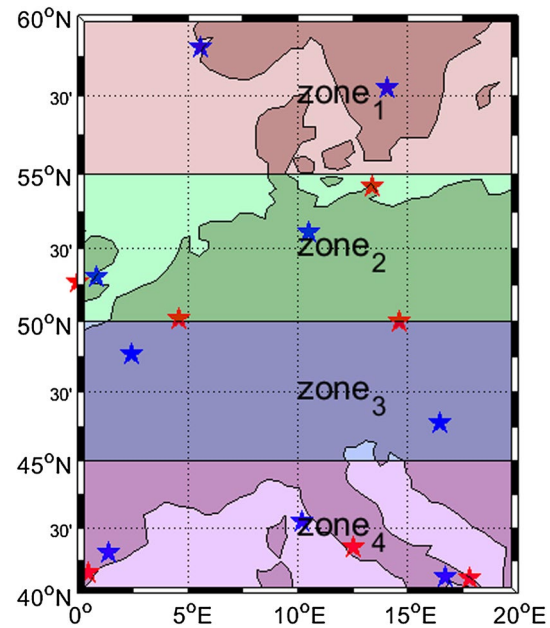


Fig. 2 Four latitudinal zones with 5° latitudinal span over Europe (40–60°N, 0–20°E) are considered, and there are 8 cells within each latitudinal zone with a spatial resolution of 2.5° in latitude and 5° in longitude. The ionosonde (red pentagram) and GNSS receiver (blue pentagram) data are used for validating the updated IRI-2016 model with respect to ionosonde Ne profiles and foF2 values, as well as GNSS-derived TEC data. The detailed information about the ionosonde and GNSS stations can be found in Tables 1 and 2, respectively

where \overline{REC}_k is the mean REC in latitudinal zone $zone_k$ for the given time moment, $k = 1, 2, 3, 4$; TEC_j are calculated with a 1-hour time resolution, and there are 8 TEC cells within each latitudinal zone (see Fig. 2); S_j is the cell's surface area at the single layer ionosphere model (SLIM) height of the ellipsoid, usually 450 km above earth's surface, and thus, R is the distance between the center of the earth and 450 km altitude, i.e., 6821 km; $\Delta\varphi$ and $\Delta\theta$ are the longitudinal and latitudinal sizes of the TEC elementary cell, usually 5° in longitude and 2.5° in latitude; θ_j is the central latitude of the TEC cell in $zone_k$. In this paper, the TEC used for calculating \overline{REC}_k (namely, $\overline{REC}_{k,GIM}$ and $\overline{REC}_{k,IRI}$) is from the CODE GIM and the IRI-2016 TEC, respectively. The hourly CODE GIM with $2.5^\circ \times 5^\circ$ spatial resolution is available from the IONEX files (<ftp://cddis.nasa.gov/pub/gps/products/ionex/>), and the IRI-2016 TEC can be calculated at the corresponding location and time for all GIM cells. As a result, we can obtain the hourly $\overline{REC}_{k,GIM}$ and $\overline{REC}_{k,IRI}$ using Eq. (1). It should be noted that the PEC contained in the CODE GIM TEC has already been deducted by using the NeQuick-2 model throughout this paper.

For the selected location and time of GIM cells, a set of IG sequences (e.g., $IG = 0, 20, 40, \dots, 200$) are used as input to the IRI-2016 model, the corresponding IRI TEC are calculated, and thus, a series of $\overline{REC}_{k,IRI}$ can be obtained based on Eq. (1). That means a set of $(IG, \overline{REC}_{k,IRI})$ pairs for the given time moment can be determined in the latitudinal zone $zone_k$. Based on our investigation, we found that it is appropriate to fit hourly $(IG, \overline{REC}_{k,IRI})$ pairs using the quadratic polynomial function (the evaluation can be found in Sect. 3.1), and as a result, the hourly mean REC $f_k(IG)$ to be fitted in each latitudinal zone $zone_k$ can be expressed as a function of the IG index.

$$f_k(IG) = a_k IG^2 + b_k IG + c_k \tag{2}$$

where a_k, b_k and c_k are the hourly coefficients over each latitudinal zone $zone_k$, and they can be estimated from a set of $(IG, \overline{REC}_{k,IRI})$ pairs mentioned above by using the least square (LS) method. Once the quadratic polynomial coefficients a_k, b_k and c_k are determined, it is easy to calculate the fitting function $f_k(IG)$ for any independent variable IG index by using Eq. (2). In other words, if a certain REC value is given as the dependent variable $f_k(IG)$, the independent variable IG can be estimated by solving the aforementioned quadratic polynomial.

To obtain the effective IG index, we assume that the $\overline{REC}_{k,GIM}$ is equal to the mean REC $f_k(IG)$ for the given time, namely $\overline{REC}_{k,GIM} = f_k(IG)$, and as a result the desired IG index can be estimated by solving the following quadratic equation,

$$\overline{REC}_{k,GIM} = a_k IG^2 + b_k IG + c_k \tag{3}$$

where $\overline{REC}_{k,GIM}$ represents the mean REC from the CODE GIM in latitudinal zone $zone_k$ for the given time moment. a_k, b_k and c_k are the quadratic polynomial coefficients, which have been determined by the aforementioned LS method; IG is the hourly IG index to be updated. Considering the actual situation of the ionosphere index (https://ccmc.gsfc.nasa.gov/modelweb/models/iri2016_vitmo.php), only the IG index estimated within $(-50, 400)$ range can be regarded as the valid final effective IG index, otherwise it is kept as the original IG12 index, which is the ionosonde-based 12-month smoothed IG index from `ig_rz.dat` file. Once the hourly IG indices for each latitudinal zone are determined, they can be used as effective inputs for the IRI-2016 to generate ionosphere parameters.

To evaluate the performance of the updated IRI-2016 model statistically in estimating foF2 (or NmF2) and TEC, we have calculated the total bias, root mean square (RMS) error and the relative difference (RD) using the following expression,

$$\left\{ \begin{aligned} \text{BIAS} &= \frac{1}{N} \sum_{i=1}^N (X_{IRI}^i - X_{obs}^i) \\ \text{RMS} &= \sqrt{\frac{1}{N} \sum_{i=1}^N (X_{IRI}^i - X_{obs}^i)^2} \\ \text{RD} &= \frac{X_{IRI}^i - X_{obs}^i}{X_{obs}^i} 100\% \end{aligned} \right. \tag{4}$$

where X_{obs}^i is the ionosonde foF2 (or NmF2) or GNSS TEC for individual stations in Tables 1 or 2, and X_{IRI}^i is the corresponding modeled foF2 (or NmF2) or TEC from either the original/updated IRI-2016, respectively. $i=1, 2, \dots, N$, and N is the total number of data samples used in the calculation. Actually, we compared IRI model outputs with ionosonde foF2 or GNSS TEC epoch by epoch for all available stations in Tables 1 or 2. The sampling interval for GNSS TEC and ionosonde foF2 we used is 30 s and 15 min, respectively.

3 Results and analysis

3.1 Effective IG indices and updated TEC values

To illustrate the feasibility of the quadratic polynomial fitting function for hourly $(IG, \overline{REC}_{k,IRI})$ pairs, we present $(IG, \overline{REC}_{1,IRI})$ pairs and corresponding fitting results

Fig. 3 The quadratic polynomial fitting $f_1(IG)$ (magenta curves) from $(IG, \overline{REC}_{1,IRI})$ pairs in zone₁ during quiet time condition (UT06:00-UT11:00, DOY075, 2015). Left axis: circle symbols is the IRI's simulated $\overline{REC}_{1,IRI}$ values calculated by Eq. (1) for $IG=0, 20, 40, \dots, 200$; red pentagrams represent the updated IG index ($IG_{upda,k}$) in latitudinal zone zone_k, $k = 1, 2, 3, 4$, and blue pentagrams represent the original IG12 index ($IG12_{orig}$) used in the IRI-2016 model. Right axis: cross-sign curves is the fitting residuals ΔREC_1 between $\overline{REC}_{1,IRI}$ and $f_1(IG)$

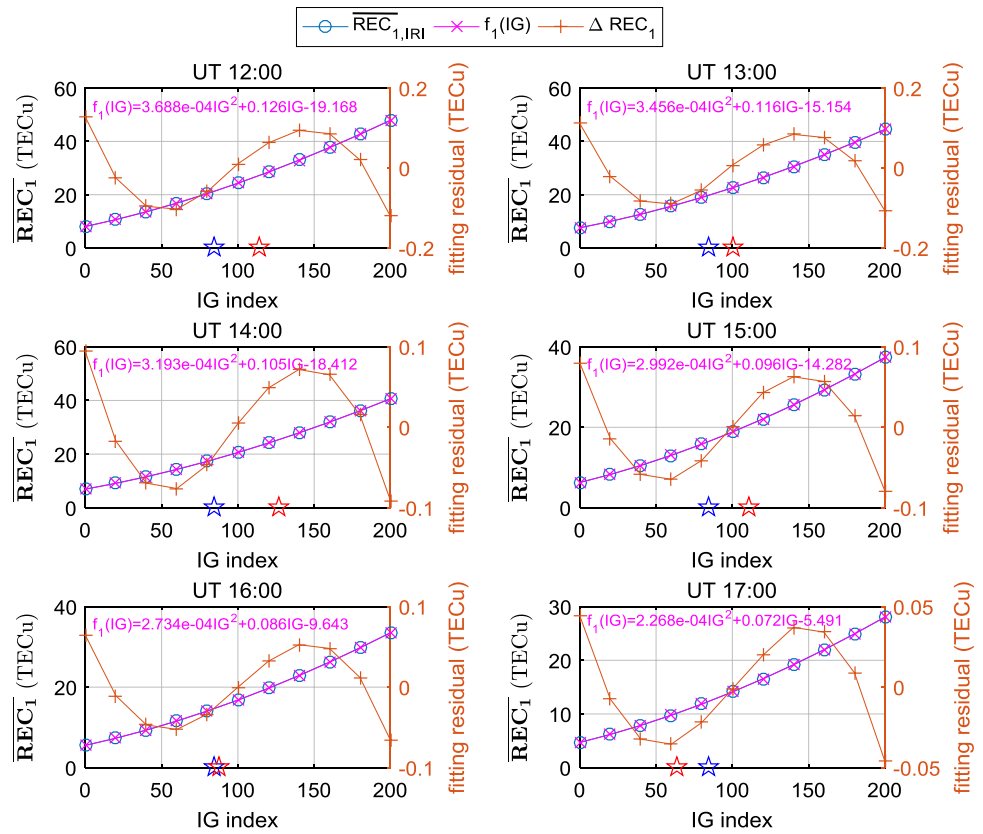
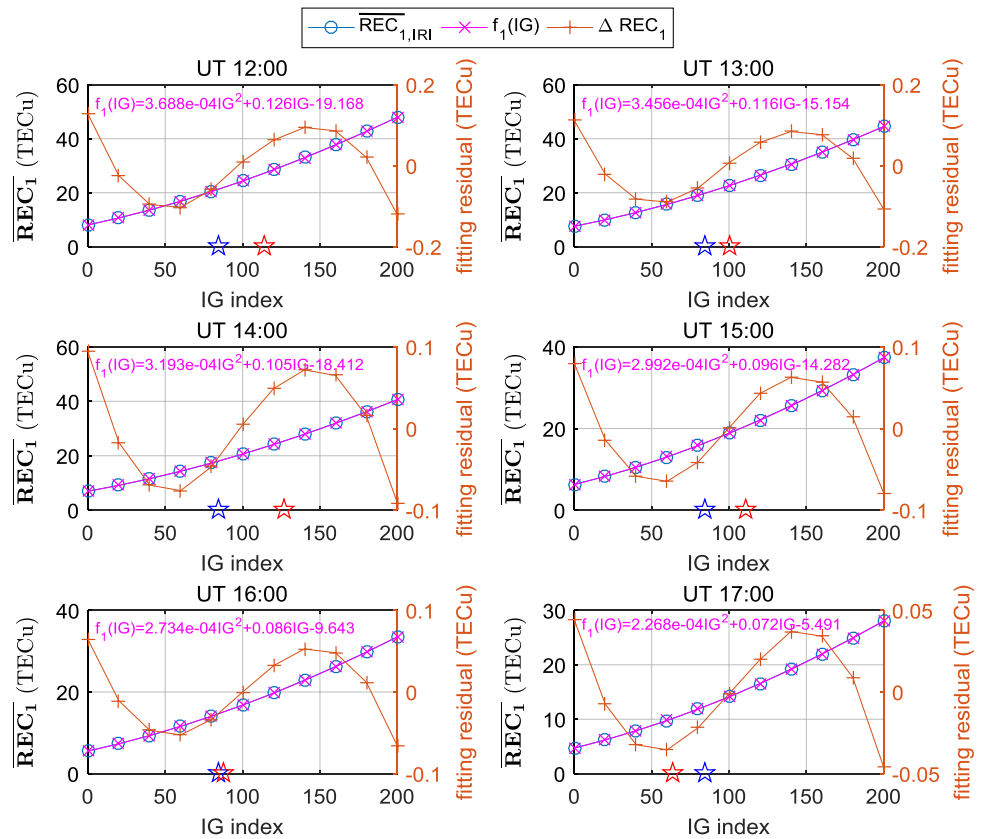


Fig. 4 Same as Fig. 3, but for the storm-time condition (UT12:00-UT17:00, DOY076, 2015). 1 TECu = 10^{16} electrons/m²



$f_1(IG)$ along with their fitting residuals over zone₁ for both quiet and storm conditions in Figs. 3 and 4, respectively. $\overline{REC}_{1,IRI}$ is the mean REC from the IRI TECs in latitudinal zone zone₁ (60°–55° in latitude); $f_1(IG)$ represents the fitted mean REC in zone₁ used by a set of (IG, $\overline{REC}_{1,IRI}$) pairs, and it is expressed as a function of IG; IG_{upda} is the updated IG index based on our method; $IG12_{orig}$ is the original IG12 index from the *ig_rz.dat* file; ΔREC_1 is the fitting residual between $\overline{REC}_{1,IRI}$ and $f_1(IG)$, namely $\Delta REC_1 = \overline{REC}_{1,IRI} - f_1(IG)$. It can be seen that $\overline{REC}_{1,IRI}$ agrees well with the fitting result $f_1(IG)$ and ΔREC_1 is extremely small under both quiet and storm conditions (fitting residuals are almost within 0.2 TECu, 1 TECu = 10¹⁶ electrons/m²). Similar results are also found in other latitudinal zones for the study period (DOY074-077, 2015). Therefore, it is appropriate to use quadratic polynomial function to fit the IRI’s hourly mean REC $f_1(IG)$ in each latitudinal zone. Once the $\overline{REC}_{k,GIM}$ is obtained from the GIM TEC, the corresponding IG_{upda} can be estimated by using Eq. (3) and being used to update the $IG12_{orig}$.

Figure 5 shows the time series of the updated IG index for each zone together with the original IG12 index during the selected period. It is shown that the updated IG indices vary considerably in different latitudinal zones, in contrast to the original IG12 index from the internal *ig_rz.dat* file. Generally, the updated IG index value is much larger during nighttime and at relatively lower latitudinal zones, indicating that it may have a greater influence on the updated IRI TEC. An interesting feature is that the updated IG indices for different latitudinal zones tend to follow a similar diurnal trend under the quiet time condition, and the IG index magnitude is higher at lower

latitudes. Compared to these updated IG indices under quiet conditions, the updated IG indices during storm days vary much more significantly, and they do not follow any regular pattern.

Figure 6 shows three mean REC (namely, $\overline{REC}_{IRI,orig}$, $\overline{REC}_{IRI,upda}$ and \overline{REC}_{GIM}) variations over different latitudinal zones, i.e., calculated from the original IRI-2016 driven by the IG12 index, updated IRI-2016 model driven by the updated IG index, and the GIM-derived TEC from CODE. It can be seen that $\overline{REC}_{IRI,orig}$ is smaller than $\overline{REC}_{IRI,upda}$ or \overline{REC}_{GIM} in each latitudinal zone, and this underestimation is much more pronounced in the lower latitudinal zones.

The curves from $\overline{REC}_{IRI,upda}$ and \overline{REC}_{GIM} are overlapped, and it is difficult to distinguish these two curves. This good agreement suggests the IRI-2016 model driven by the updated IG index is able to reproduce the observed TEC values when the GIM-derived TEC is ingested into the IRI-2016, and this match is especially significant during the storm time. During storm time, $\overline{REC}_{IRI,orig}$ and $\overline{REC}_{IRI,upda}$ have distinctly different behaviors in each latitudinal zone, and their difference (ΔREC) can even exceed 10 TECu, especially for the low latitudinal zones. This difference is expected to some extent since most empirical ionosphere models poorly describe the short-time ionospheric features during storms. Comparing the ΔREC (in the right axis of Fig. 6) with the updated hourly IG index (in the left axis of Fig. 5), it is interesting to note that the hourly ΔREC between $\overline{REC}_{IRI,orig}$ and $\overline{REC}_{IRI,upda}$ in each latitudinal zone has a similar trend to the updated hourly IG index shown in Fig. 5, and this similarity is particularly pronounced during storm hours. This suggests that the IRI-2016 model is able to yield good TEC results for both quiet and storm conditions

Fig. 5 Updated hourly IG indices ($IG_{upda,k}$) for different latitudinal zones zone_k, $k = 1, 2, 3, 4$, and original 12-month smoothed IG index ($IG12_{orig}$) for the studied periods

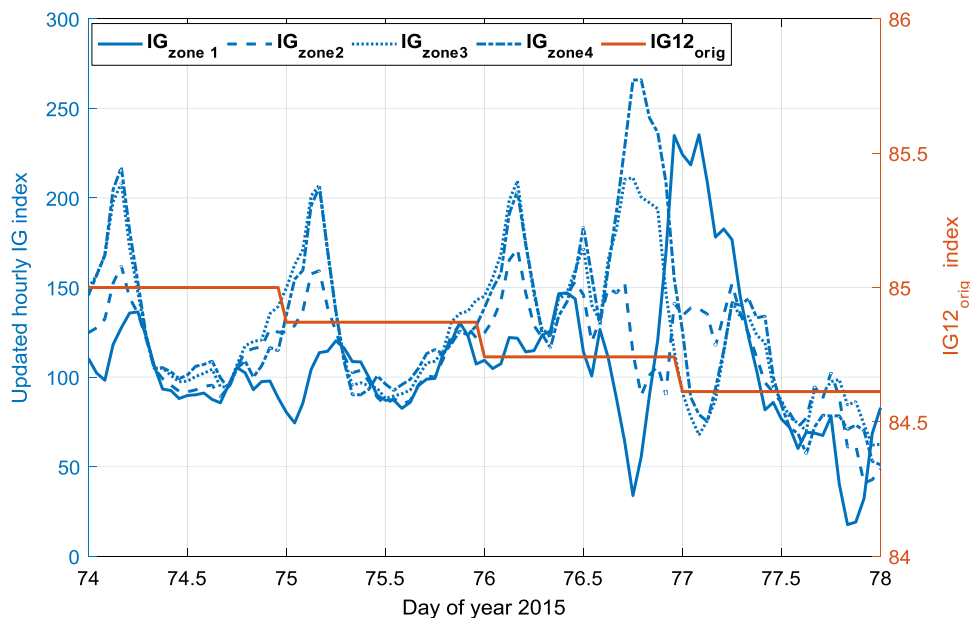
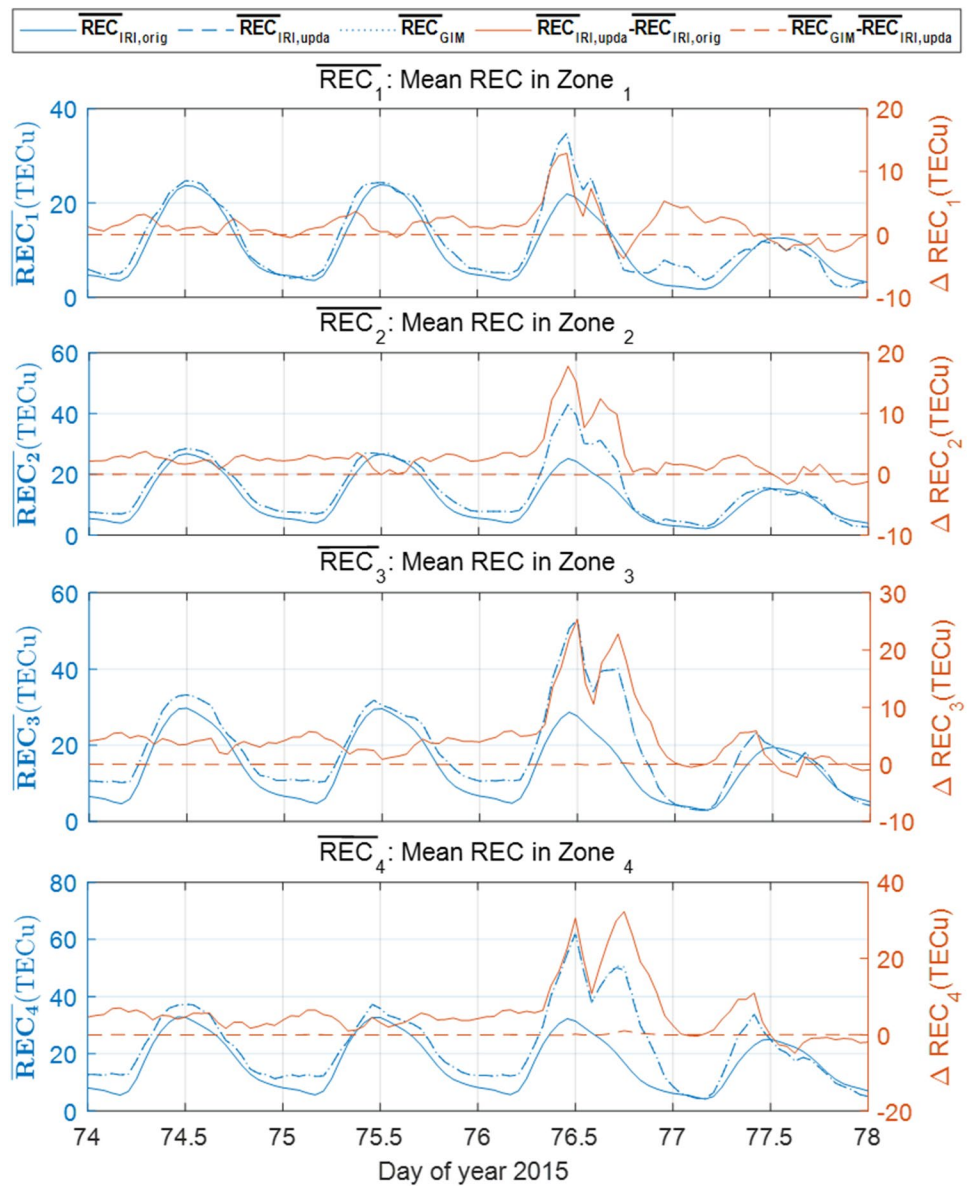


Fig. 6 Hourly mean REC variations ($\overline{REC}_{IRI,orig}$, $\overline{REC}_{IRI,upda}$ and \overline{REC}_{GIM}) over different latitudinal zones calculated from IRI-2016 with original IG12 indices, IRI-2016 model with updated IG indices, and CODE GIM TEC values (left axis); and they are determined by Eq. (1). Corresponding differences ΔREC between them are computed by $\overline{REC}_{IRI,upda}$ minus $\overline{REC}_{IRI,orig}$, or \overline{REC}_{GIM} minus $\overline{REC}_{IRI,orig}$ (right axis)



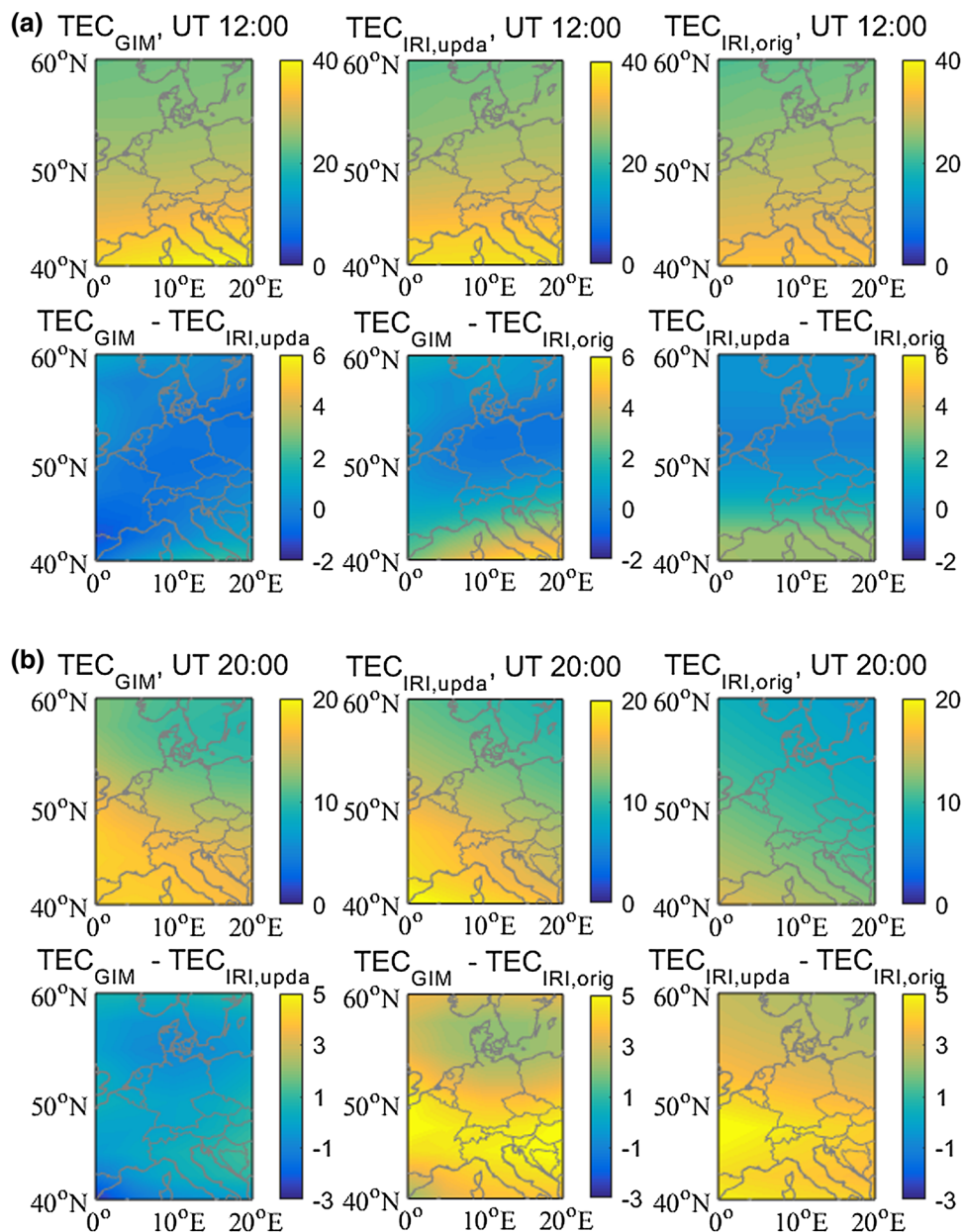
through modification of the IG index based on the GIM-derived TEC.

It is known that the hourly CODE GIM-derived TEC map has a spatial resolution of 2.5° in latitude and 5° in longitude, so the updated or original IRI TEC can be calculated at the corresponding location and time for corresponding CODE GIM cells when IRI-2016 is driven by the IG_{upda} and $IG_{12,orig}$, respectively. Figure 7 shows two-dimensional TEC maps over Europe (from left to right: GIM-derived TEC, IRI-updated TEC and original IRI TEC, along with their differences in the second row) for the quiet condition (DOY076, 2015). When the effective IG index is used to drive the IRI model, the resultant IRI-updated TEC over Europe are closer to the GIM-derived TEC than the original IRI TEC, indicating that it is effective to improve IRI based on the updated IG index. Generally, it is observed that the

difference between the updated IRI TEC and original IRI TEC is always positive, and the difference value is much larger at lower latitudes, suggesting that the original IRI-2016 model underestimates TEC and that the updated TEC improvement is much more pronounced at relatively lower latitudes.

Figure 8 is similar to Fig. 7, but for the storm condition. Compared to the GIM-derived TEC, the updated IRI-2016 TEC is significantly improved during the storm condition, while a large underestimation is observed from the original IRI TEC values. The absolute difference between the GIM-derived TEC and the IRI-updated TEC during daytime and nighttime is about 3 TECu and 5 TECu, respectively. However, the absolute difference between the GIM-derived TEC and the original IRI TEC reaches 30 TECu.

Fig. 7 Two-dimensional TEC maps along with their differences in **a** the daytime (UT 12:00) and **b** the nighttime (UT 20:00) for the quiet condition (DOY075, 2015). Top panel: TEC_{GIM} , $TEC_{IRI,upda}$ and $TEC_{IRI,orig}$; bottom panel: TEC_{GIM} minus $TEC_{IRI,upda}$, TEC_{GIM} minus $TEC_{IRI,orig}$, and $TEC_{IRI,upda}$ minus $TEC_{IRI,orig}$; where TEC_{GIM} is the GIM-derived TEC from CODE, $TEC_{IRI,upda}$ is IRI TEC driven by updated hourly IG indices (IG_{upda}), and $TEC_{IRI,orig}$ is IRI TEC driven by original IG12 indices ($IG12_{orig}$). The spatial resolution is 2.5° in latitude and 5° in longitude, and the bilinear interpolation is used to construct these maps. Unit: TECu



It is also noticed that the difference in magnitude between the updated TEC and the original TEC during the storm condition is much larger than that during the quiet time (see Figs. 7 and 8), indicating that the improvement in the updated TEC is generally better under storm conditions compared to that under the quiet time. Overall, the updated IRI-2016 with effective IG indices has significantly improved TEC performances and can help to capture the ionospheric dynamics, particularly during the storm days.

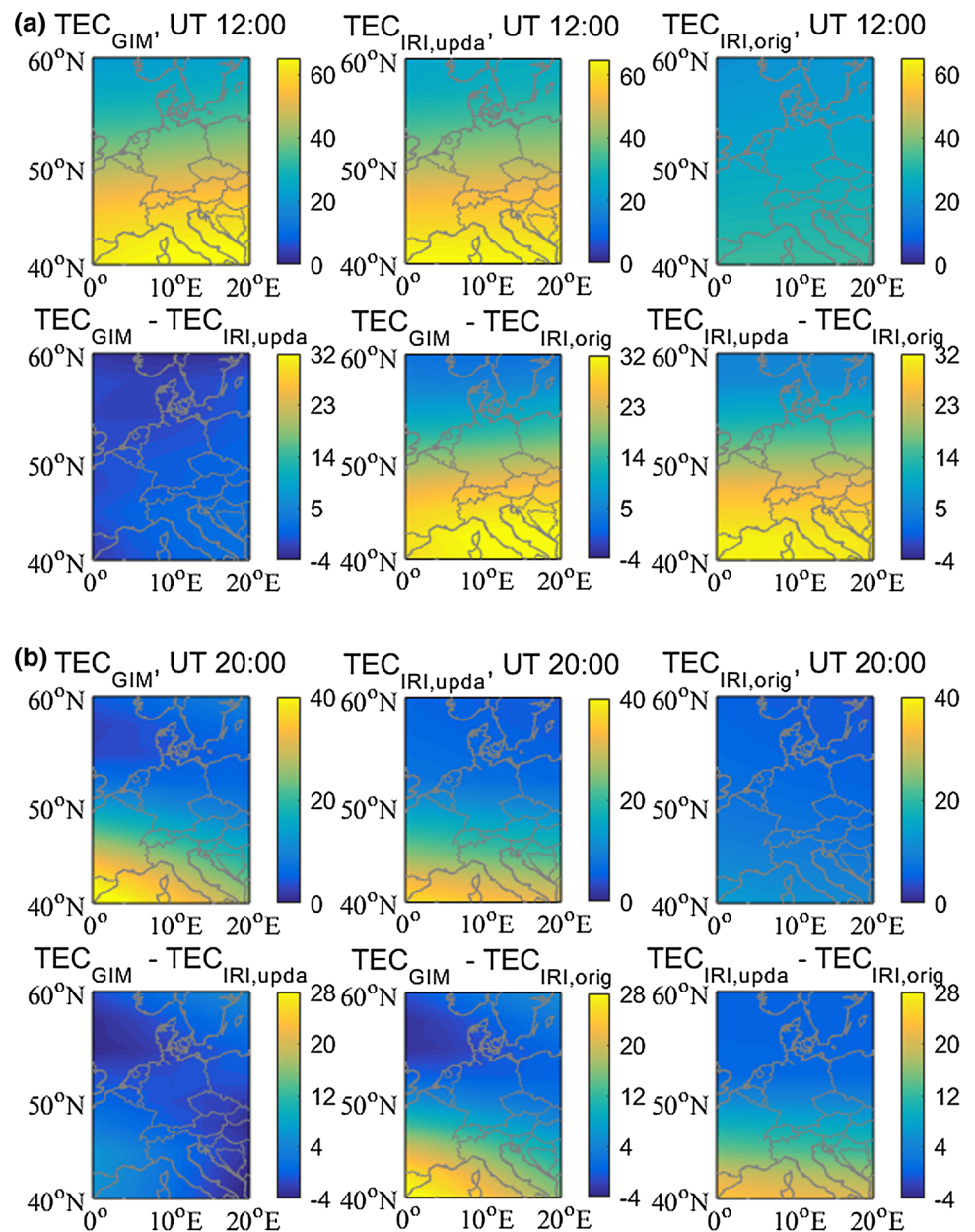
3.2 Cross-validation of the ingestion technique

To test the performance of the proposed ingestion technique, the retrieved parameters from the updated/original IRI-2016 model are evaluated with respect to the COSMIC/ionosonde electron density profiles, ionosonde foF2 values, and GNSS TEC data for both quiet and storm conditions.

3.2.1 Electron density (Ne) profile and foF2 results

To validate the Ne output from the updated IRI-2016 model, we compared our updated Ne profiles with those from the original IRI-2016 model and the COSMIC radio occultation data. The COSMIC Ne profiles are available at CDDAC

Fig. 8 Similar to Fig. 7, but for the storm condition (DOY076, 2015)



‘ionPrf’ products (<http://cdaac-www.cosmic.ucar.edu/cdaac/>), and their accuracy is generally about 10^4 – 10^5 cm^{-3} . As shown in Fig. 9, three different time cadences are shown. In our case, we only select COSMIC data when the COSMIC tangent point trajectory is entirely within the research area, and the spatial coverage for the COSMIC tangent point trajectory is within $5^\circ \times 5^\circ$ in latitude and longitude to avoid arcs expanding too broad areas. With the exception of the Ne profile in (a) at 20:42 UT on March 15, 2015, the retrieved COSMIC Ne profile shape matches better with the Ne profile from the updated IRI-2016 than that from the original IRI-2016. It should be noted that the Ne estimations from both the original IRI-2016 and the updated IRI-2016 do not match well with the COSMIC profile below 200 km, where

the Ne values are sometimes negative (such as at 16:48 UT on March 18, 2015). This is because of a known issue that the Ne profile from COSMIC is not accurate enough at the bottom ionosphere due to the unreasonable spherical symmetry assumption used when inverting the electron densities (Ne), which degrades the Ne inversion performance in low altitudes and at low-latitude regions (Lei et al. 2007; Yue et al. 2011; Pedatella et al. 2015). In terms of NmF2, it can be seen that the updated IRI NmF2 are closer to the COSMIC NmF2 than the original IRI NmF2 in (b) at 11:27 UT on March 16, 2015, and (c) 16:48 UT on March 18, 2015, though the comparison is poor in (a). This significant discrepancy is probably due to the large horizontal coverage

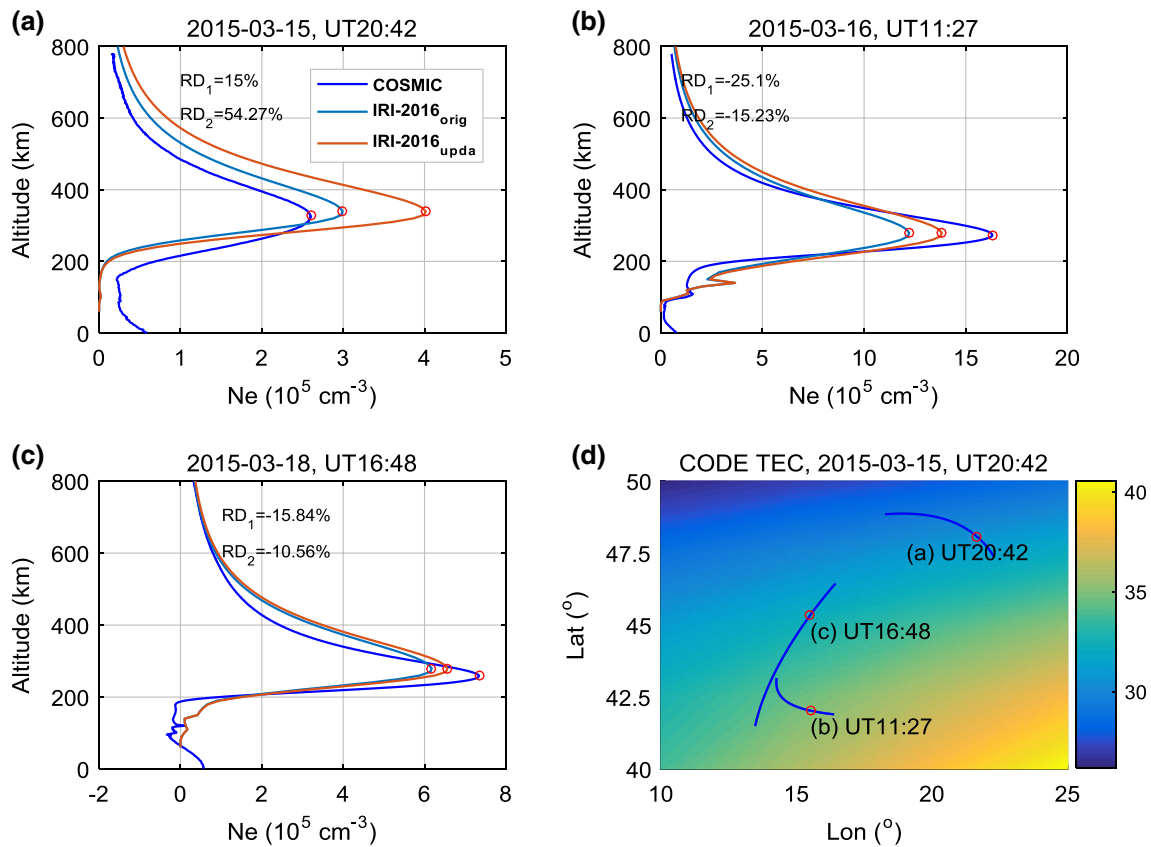


Fig. 9 a–c Ne altitude profile comparisons among data retrieved from the COSMIC radio occultation, the IRI-2016 with the original IG12 index, and the IRI-2016 with updated hourly IG index, when the COSMIC data were available within the European sector. The COSMIC Ne altitude profiles are not rigorously vertical because each altitude profile is based on measurements obtained within a short time period, while the IRI-2016 Ne profiles in our case are calculated at

the longitude and latitude where the COSMIC NmF2 were obtained, which are shown as red circles. **d** The COSMIC occultation satellite tangent point (blue curves) for the retrieval of Ne profiles superimposed on CODE TEC map (March 15, 2015, 20:42 UT). RD1 and RD2 in each panel are the relative differences in NmF2 between the original/updated IRI model and the COSMIC measurements

of the tangent point trajectory (see Fig. 9d) and the assumption of spherical symmetry in retrieving the electron density.

We also compared the original and updated Ne profiles with ionosonde data for both the quiet condition (DOY075) and the storm condition (DOY076) in Figs. 10 and 11. In order to quantify the NmF2 performance for both quiet and storm conditions, relative differences (RD) between the original/updated IRI-modeled and the ionosonde-based NmF2 are calculated, and the NmF2 improvement percentages for Figs. 10 and 11 are calculated by $|\text{RD}_1|$ minus $|\text{RD}_2|$, where RD is computed by Eq. (4). As shown in Fig. 10, the bottom-side (below 250 km) Ne profiles generated by the updated IRI-2016 during the quiet time are very close to the ionosonde measurement, though both the original and the updated IRI-2016 estimations show large discrepancies compared to the ionosonde topside Ne profile. It is widely recognized that the ionosonde bottom-side electron density is very reliable, which has been confirmed by incoherent scatter data (Huang and Reinisch 1996). In the ionosonde

topside ionosphere, an extrapolated method is used for upper missing trace points to maintain the consistent frequency (<http://ulcar.uml.edu/~iag/SAO-4.3.htm>). Therefore, it is difficult to know the real Ne profiles in the topside ionosphere from the ionosonde measurement.

Figure 11 is similar to Fig. 10 but for the storm condition. Compared to the quiet time condition, the Ne profile differences between the original IRI-2016 and the updated IRI-2016 are much larger in the storm time, and the updated IRI-2016 Ne values agree better with the values from ionosonde, in particular in the bottom-side ionosphere. Generally, when the IRI-2016 model is driven by the hourly updated IG index, there are obvious NmF2 improvements as reflected by the percentage change from RD1 to RD2. The mean NmF2 improvement percentage for these ionosonde stations is about 17.19%, and the improvement percentage under the storm condition (28.10%) is better than that in the quiet condition (6.27%). It should be noted that there are

Fig. 10 Ne profile comparisons among the ionosonde, the original IRI-2016, and the updated IRI-2016 in **a** the daytime (UT 10:00) and **b** the nighttime (UT 18:00) for the quiet condition (DOY075, 2015). RD1 and RD2 in each panel are the relative differences in NmF2 between the original/updated IRI model and the ionosonde measurements

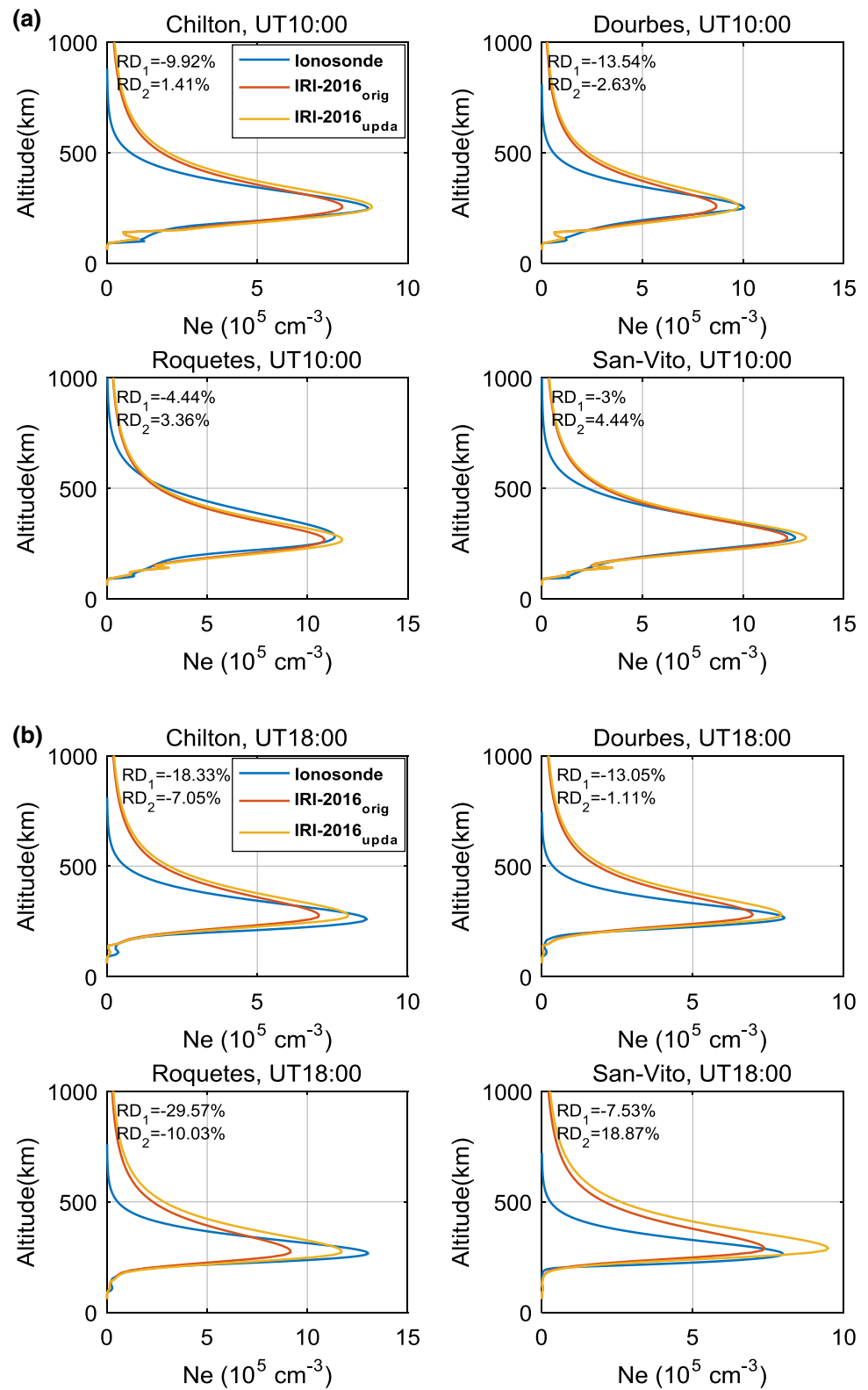
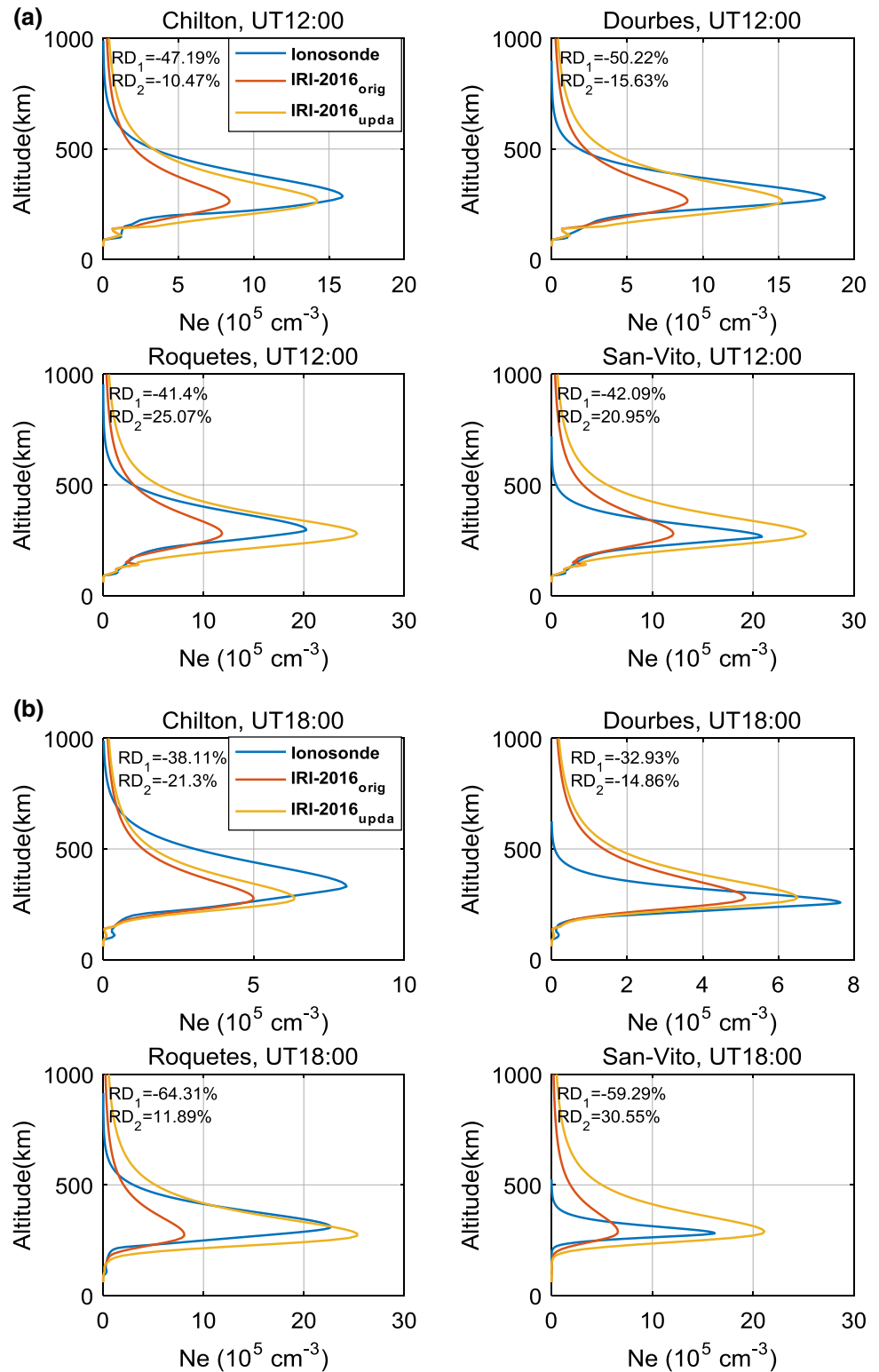


Fig. 11 Similar to Fig. 10, but for the storm time. **a** The daytime (UT 12:00) and **b** the nighttime (UT 18:00) for the storm condition (DOY076, 2015)



minor NmF2 degrades only at the San Vito station during the quiet time.

Based on the above comparisons, the performance of the updated IRI-2016 model driven by the improved IG index is

significantly improved, in terms of the bottom-side electron density profile and the NmF2 values.

The foF2 is one of the most useful output parameters that can be generated by the IRI-2016 model, so we also performed a comparison between the foF2 values

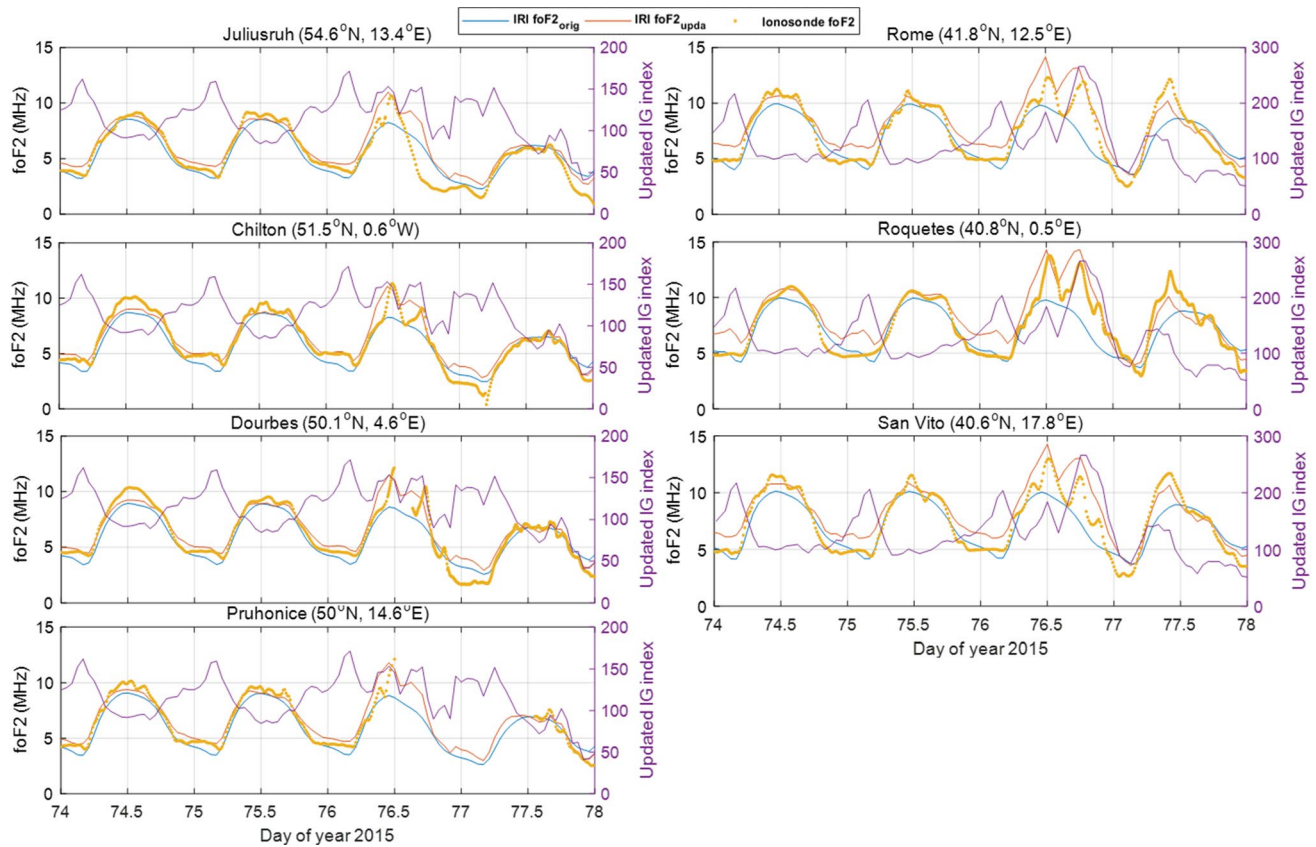


Fig. 12 Comparisons between foF2 values as measured by ionosondes and calculated by original/updated IRI-2016. The right axis represents the hourly updated IG indices for corresponding latitudinal zones used in IRI-2016 to generate the foF2 values

measured by ionosondes and calculated by the original/updated IRI-2016 model over the European sector in Fig. 12. In addition, the hourly updated IG index values are also shown as a purple curve in this figure.

In general, the IRI-updated foF2 curves show, as expected, better agreement with the measured foF2 values over different stations for both quiet days and more pronounced agreement for severe storm days. For example, such agreement is especially obvious at the double-peak structure at relatively lower latitudes during DOY076. That means that the updated IRI-2016 is very useful in describing the foF2 values and is able to better capture the ionospheric dynamics and abnormal structures during geomagnetic storms than the original IRI-2016.

On the other hand, compared to the original IRI-2016 foF2, the updated IRI-2016 overestimates the nighttime foF2, especially at relatively lower latitudes (such as Rome, Roquetes and San Vito). This overestimation is directly associated with larger IG index used in the updated IRI-2016 model. Possible explanations of this performance could be attributed to two aspects: (1) The improper SLIM height used at the nighttime in determining the IG index: The

ionosphere effective height (IEH) generally represents the mean altitude of maximum electron density, which typically ranges from 300 to 500 km above the earth surface (Lanyi and Roth 1988; Mannucci et al. 1998), and the IEH is found to have clear diurnal/seasonal/latitudinal dependences (Birch et al. 2002; Nava et al. 2007; Brunini et al. 2011; Li et al. 2018). In our case, the SLM height (450 km) is regarded as the IEH, but 450 km may not be appropriate in different locations during nighttime. This means the unreasonable nighttime SLM height (450 km) will introduce significant errors into nighttime GIM-derived TEC and surface area S_f , thus resulting in the larger nighttime IG index. Therefore, the updated nighttime IG index used in IRI-2016 may lead to the foF2 overestimations. (2) The underestimation of the nighttime PEC calculated from the NeQuick-2 model: The NeQuick-2 model may underestimate PEC with several TECu above 500 km, which is directly related to the simplified semi-Epstein extension of the topside density profile toward GNSS altitude used in the NeQuick-2 model (Cherniak and Zakharenkova 2016). Moreover, this PEC underestimation may be much more significant during the nighttime than that during the daytime, because PEC percentage

contribution to TEC is larger on the nightside compared to that on the dayside (Yizengaw et al. 2008; Klimentko et al. 2015). These mean that the nighttime GIM-derived TEC can still be overestimated, even though the nighttime PEC contribution contained in the GIM-derived TEC has been removed to a certain degree by using the NeQuick-2 model. Therefore, the absolute difference between the GIM-derived TEC and the original IRI TEC is much larger during nighttime than that during daytime, thus resulting in larger retrieved nighttime IG indices. As a result, the nighttime foF2 from the updated IRI model driven by the updated nighttime IG index is likely overestimated. Further studies should focus on improving the PEC estimation and thus nighttime IG index.

3.2.2 Ionospheric TEC results

In this section, we compare the ionospheric vertical TEC (vTEC, hereafter referred to as TEC) parameters from the original/updated IRI-2016 models and the GNSS observations from EUREF Permanent Network (EPN, blue pentagrams in Fig. 2) in Fig. 13. In this study, the GNSS TEC

over a particular station is determined using the regularized estimation (Reg-Est) algorithm, which is based on a cost function minimization and a high-pass penalty filter (Arikan et al. 2003, 2004, 2007, 2008; Nayir et al. 2007; Sezen et al. 2013). It should be noted that the PEC from 2000 to 20,200 km contained in the GNSS-based TEC has been subtracted by using the NeQuick-2 model. Therefore, the GNSS-based TEC integral height range in our case is consistent with that from the IRI-derived TEC, namely 60–2000 km.

As shown in Fig. 13, when the updated hourly IG index is used to drive the IRI-2016 model, the resulted TEC have better agreements with the GNSS TEC values than the original IRI TEC for both quiet and storm conditions. The improvement is particularly obvious during the nighttime and in the main phase of the storm time, while both the updated and original IRI-2016 models yield TEC well in the recovery phase of the geomagnetic storm (the afternoon and nighttime of DOY077). During quiet times, the TEC difference between the GNSS-based/IRI-updated TEC and the original IRI TEC during the nighttime is always larger than that during the daytime, which is responsible for the larger updated

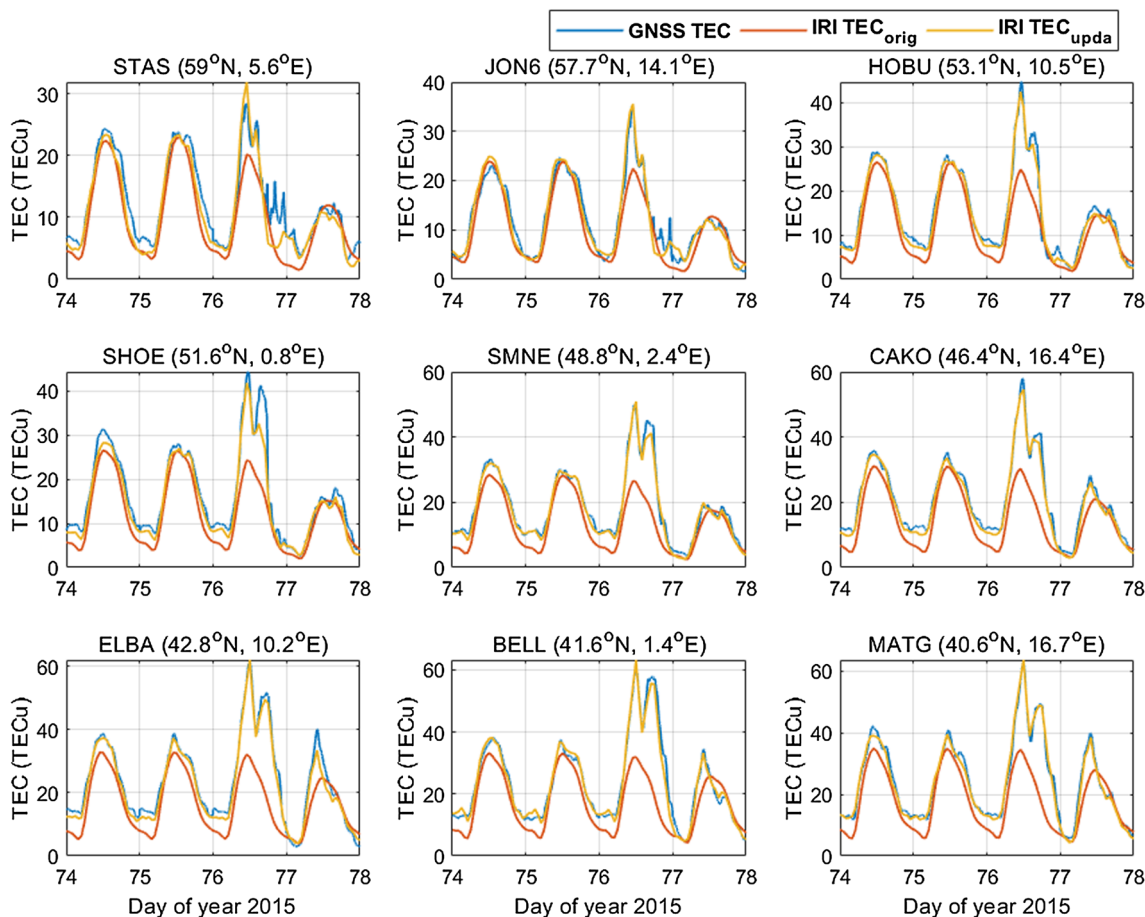


Fig. 13 IRI-2016 TEC validation with respect to GNSS TEC data from EPN

IG index during nighttime, as shown in Fig. 5, and thus results in the large nighttime updated IRI-2016 TEC values compared to the original IRI-2016 TEC outputs. Additionally, an outstanding feature in Fig. 13 is that the GNSS TEC and the updated IRI-2016 TEC exhibit irregular variability over all stations during the storm time. For instance, there is a double-peak structure (one on the dayside and the other on the duskside) and positive TEC responses in the main phase, while the negative ionospheric storms are observed during the recovery phase in early DOY077.

In terms of the storm-time physical drivers, the negative storm during the recovery phase is usually dominated by the thermosphere neutral composition changes related to the storm circulation theory (Astafyeva et al. 2015; Nayak et al. 2016), whereas the positive ionospheric responses can be due to several competing physical mechanisms, such as storm-time equatorward thermospheric winds, prompt penetration electric fields and equatorial super fountain, or a combination of them (Huang et al. 2005; Crowley et al. 2006; Danilov 2013; Foster et al. 2005; Zou et al. 2013).

3.3 Statistical assessment

Figure 14 shows histogram of calculated TEC errors as a function of TECu in the study periods (DOY074-077, 2015) for nine EPN stations (see Table 2). Red/green refers to the difference between the original/updated IRI-2016 modeled and the GNSS-based TEC. It is clear that the updated

TEC residual distributions for both daytime and nighttime are much more concentrated around zero. The TEC BIAS/RMS of the updated IRI-2016 reduces from $-5.34/8.37$ to $-0.53/1.74$ TECu during the daytime, and from $-4.30/6.76$ to $-1.04/1.80$ TECu during the nighttime. It is also evident that overall the TEC is improved approximately by 19%, and the RD reduces from -18.74 to -2.48% during the daytime and from -29.78 to -8.39% during the nighttime. This means that the TEC improvement during the nighttime is better than that during the daytime, which is likely due to the underestimation of the original IRI-2016 TEC during the nighttime.

To make a more comprehensive validation under different geomagnetic conditions, we expanded the period from four days to one month covering DOY060-090 (March 1-31), 2017. The bottom panel of Fig. 15 shows daily F10.7 and daily mean Dst indices for one month, which covers different levels of geomagnetic activities. The top and middle panels of Fig. 15 show the daily BIAS and RMS results from the original and updated IRI TEC with respect to the observed GPS TEC, respectively. It can be seen that the daily BIAS and RMS of the updated IRI TEC are much smaller than that driven by the original IG12 indices: the averaged TEC BIAS/RMS reduces from $-4.23/6.09$ to $-0.34/2.31$ TECu; thus, we can conclude that the updated IRI-2016 model is effective in generating TEC for different geomagnetic levels. In addition, the improvement in the updated IRI-2016 model is the most significant during storm time. This is because the

Fig. 14 TEC residual distribution for original IRI (red histogram) and updated IRI (green histogram) with respect to nine EPN stations from Table 2 in the study period (DOY074-077, 2015). Statistical indices BIAS, RMS, and RD are also included

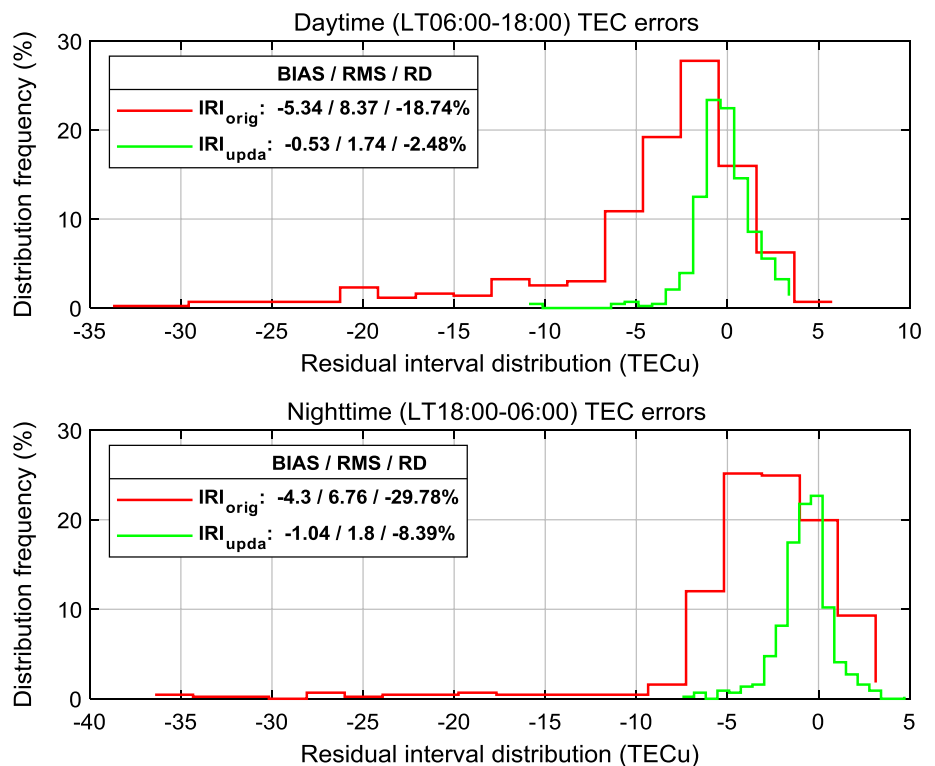
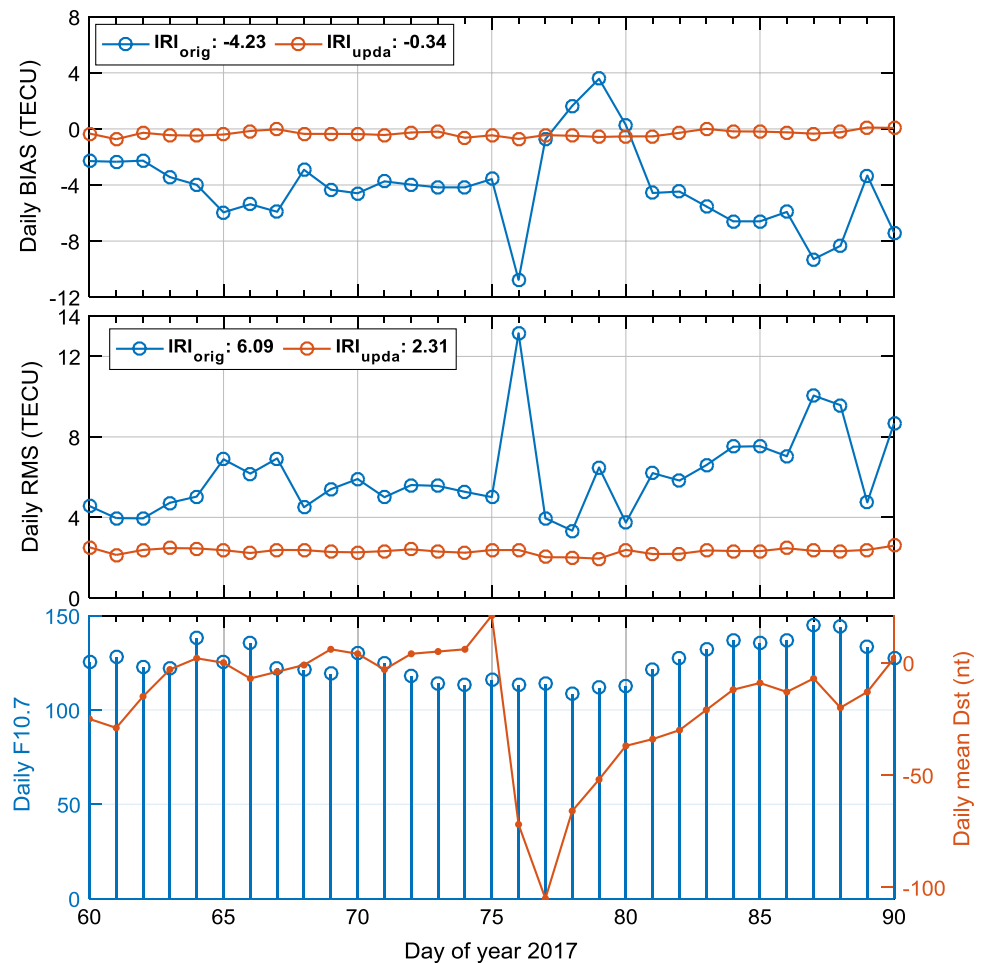


Fig. 15 Daily TEC BIAS and RMS for the original and updated IRI with respect to nine EPN stations during DOY060-090 (March 1–31), 2015



original IRI-2016 model actually has no response to ionosphere storms even though the IRI storm mode is turned on, whereas the updated IRI is able to reflect short-term ionospheric dynamics, particularly under storm conditions.

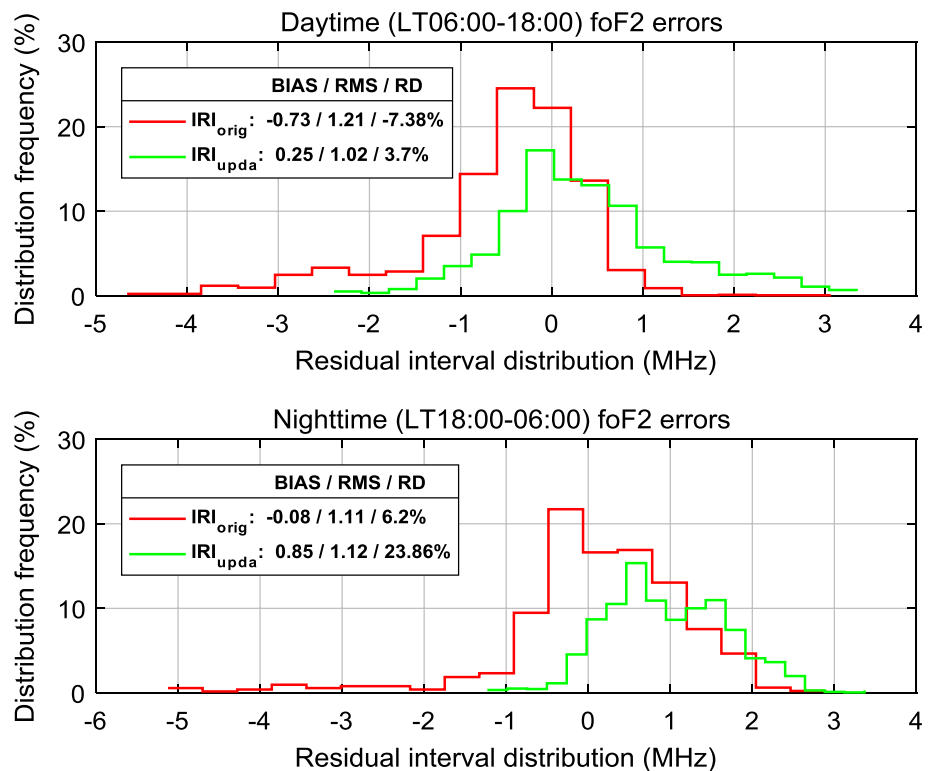
Figure 16 shows the statistical comparison of seven ionosondes foF2 measurements (see Table 1) with those calculated using the original IRI-2016 model (red) and the updated IRI-2016 model (green) during DOY074-077, 2015. Generally, the foF2 residual distributions are more symmetric and centered when the updated IRI-2016 model is used. The original IRI-2016 model is clearly biased toward underestimating the foF2.

In terms of BIAS/RMS/RD, the updated IRI-derived foF2 performances for the daytime and the nighttime are somewhat different. During the daytime, it appears that the foF2 estimations based on the updated IRI-2016 model have lower BIAS and RMS compared to the original IRI-2016 model (BIAS/RMS reduces from $-0.73/1.21$ to $0.25/1.02$ TECu), and the foF2 improvement represented by RD is almost 4%

(RD decreases from -7.38 to 3.7%). This means the updated IRI-2016 model is able to better describe the daytime foF2 values. However, it seems that the updated IRI-2016 overestimates foF2 during the nighttime (BIAS increases from -0.08 to 0.85 TECu), and the degradation performance is generally 18% (RD increases from 6.2 to 23.86%). Actually, this IRI-derived foF2 overestimation is directly associated with the larger updated IG indices during the nighttime used to update the IRI-2016 model: The difference between the GIM-derived TEC and the original IRI TEC during nighttime is larger than that during daytime (see Figs. 7 and 8), thus resulting in relatively larger updated IG index during nighttime. As a result, the nighttime foF2 is generally overestimated when using the updated IRI-2016 model.

Overall, the updated IRI-2016 model has good performance in estimating TEC/foF2 parameters for both quiet and storm conditions, though further study should be focused on improving the nighttime foF2 values.

Fig. 16 The foF2 residual distribution for original IRI (red histogram) and updated IRI (green histogram) with respect to six ionosonde stations in Table 1 in the study periods (DOY074-077, 2015). Statistical indices BIAS, RMS, and RD are also included



4 Summary and conclusions

In this study, we developed effective hourly IG index to update the IRI-2016 model by ingesting GIM-derived TEC over the European sector (40–60°N, 0–20°E) into the IRI-2016 model, and the updated IRI-2016 model reproduced ionospheric parameters were externally evaluated with the COSMIC/ionosonde Ne profiles, individual GNSS TEC, and ionosonde foF2 data for both quiet and storm conditions. As expected, the updated IRI-2016 model in general shows a better performance in estimating the Ne/TEC/foF2 parameters. This updated model was able to reflect short-term ionospheric dynamics, especially under storm conditions.

1. The hourly IG index for each latitudinal zone is determined under the assumption that $\text{REC}_{k,\text{GIM}}$ equals $f_k(\text{IG})$ for the given time. It is worth noting that the updated IG index under quiet time condition for different latitudinal zones tends to follow a similar diurnal trend, and that the IG index magnitude is higher at lower latitudes. Furthermore, the updated IG index during storm days varies much more significantly than that under quiet time condition and do not follow the diurnal pattern. When the effective IG index is used to drive the IRI-2016 model, the updated IRI-2016 model yields improved TEC values for both quiet days and more pronounced results for storm days, while the original IRI-2016 model underestimates TEC, especially at relatively lower latitudes.

This indicates the updated hourly IG index based on the GIM-derived TEC is a promising parameter to update the IRI-2016 model.

2. To test our proposed ingestion technique, the retrieved parameters from the updated IRI-2016 model are investigated with respect to the COSMIC/ionosonde electron density profiles, ionosonde foF2 values and GNSS TEC data. The updated IRI-2016 leads to better Ne profiles during daytime when compared to available COSMIC data. However, due to the fact that the bottom-side Ne profile from COSMIC is not accurate enough, so we also compared the modeled Ne profiles to ionosonde measurements, which provide reliable bottom-side electron density. As expected, the updated IRI-2016 performance in estimating the electron density shows better agreement with ionosonde measurements under the quiet condition, especially for the bottom-side Ne profiles and NmF2 values as well as the storm-time Ne profiles, and these good agreements are obviously due to the updated hourly IG index used to drive the IRI-2016 model.
3. When the updated IRI-derived TEC is compared to external GNSS-based TEC from EPN, it is found that the TEC residual distributions for both the daytime and nighttime are much more concentrated around zero. The TEC improvement is around 19%. Moreover, the TEC improvement during the nighttime is better than that during the daytime. Also, a double-peak structure can

be successfully captured from the IRI-updated TEC and foF2 parameters in the storm-time DOY076.

4. In terms of foF2 parameters, the improvement with respect to ionosonde measurements during the daytime is approximately 4% on the whole, and especially better foF2 agreements can be found for the storm condition. However, it seems that updated IRI-2016 overestimates foF2 parameters during the nighttime, and the degradation performance is generally 18%. Actually, this IRI-derived nighttime foF2 overestimation is directly associated with the larger updated IG indices during the nighttime used in IRI-2016, and we suggest two possible explanations for the nighttime foF2 degradation: (1) The improper SLIM height used at the nighttime in determining the IG index; and (2) the underestimation of the nighttime PEC calculated from NeQuick-2 model. Future studies should focus on further improving the nighttime IG index.
5. Our method, even though promising, has been tested by considering only the European region. Since the ionosphere may show distinctive behaviors at different latitudes, we will expand the proposed method to the global ionosphere specification in the future. Moreover, considering the computational burden and time it takes to generate the new set of the IG indices, we intend to release the updated IG indices and open them to all users if needed.

Acknowledgements This work was supported by the National Key Research and Development Program of China (No. 2016YFB0501803), the National Natural Science Foundation innovation research group project (No. 41721003). S. Zou acknowledges NSF AGS 1400998. The GNSS data are archived from the EUREF Permanent Network (<http://epncb.oma.be/>), the ionosonde data were downloaded from the NOAA website (<ftp.ngdc.noaa.gov/ionosonde/data/>), and the IONEX files that contain the GIM-derived TEC are available at <ftp://cddis.nasa.gov/pub/gps/products/ionex/>. The COSMIC radio occultation data are available at CDDAC (<http://cdaac-www.cosmic.ucar.edu/cdaac/>). The geomagnetic/solar activity indices data are obtained from the NASA Goddard Space Flight Center (<https://spdf.gsfc.nasa.gov/index.html>).

Author contributions All authors made great contributions to the work. Yibin Yao and Shasha Zou designed the research; Lei Liu and Jian Kong performed the research; Lulu Shan, Changzhi Zhai, Cunjie Zhao and Youkun Wang analyzed the data; and Lei Liu and Shasha Zou wrote the paper.

References

Aa E, Ridley AJ, Huang W, Zou S, Liu S, Coster AJ, Zhang SR (2018) An ionosphere specification technique based on data ingestion algorithm and empirical orthogonal function analysis method. *Space Weather*. <https://doi.org/10.1029/2018SW001987>

- Afraimovich EL, Astafyeva EI, Oinats AV et al (2008) Global electron content: a new conception to track solar activity. *Ann Geophys: Atmos Hydrospace Sci* 26(2):335
- Araujo-Pradere EA, Fuller-Rowell TJ, Codrescu MV (2002) STORM: An empirical storm-time ionospheric correction model 1: Model description. *Radio Sci* 37(5):3-1-3-12
- Arikan F, Erol CB, Arikan O (2003) Regularized estimation of vertical total electron content from global positioning system data. *J Geophys Res: Space Phys*. <https://doi.org/10.1029/2002ja009605>
- Arikan F, Erol CB, Arikan O (2004) Regularized estimation of vertical total electron content from GPS data for a desired time period. *Radio Sci*. <https://doi.org/10.1029/2004rs003061>
- Arikan F, Arikan O, Erol CB (2007) Regularized estimation of TEC from GPS data for certain midlatitude stations and comparison with the IRI model. *Adv Space Res* 39(5):867–874. <https://doi.org/10.1016/j.asr.2007.01.082>
- Arikan F, Nayir H, Sezen U, Arikan O (2008) Estimation of single station interfrequency receiver bias using GPS-TEC. *Radio Sci* 43(4):RS4004. <https://doi.org/10.1029/2007rs003785>
- Astafyeva E, Zakharenkova I, Förster M (2015) Ionospheric response to the 2015 St. Patrick's Day storm: a global multi-instrumental overview. *J Geophys Res Space Phys* 120:9023–9037. <https://doi.org/10.1002/2015JA021629>
- Bilitza D, Bhardwaj S, Koblinsky C (1997) Improved IRI predictions for the GEOSAT time period. *Adv Space Res* 20:1755–1760. [https://doi.org/10.1016/S0273-1177\(97\)00585-1](https://doi.org/10.1016/S0273-1177(97)00585-1)
- Bilitza D, McKinnell L-A, Reinisch B, Fuller-Rowell T (2011) The international reference ionosphere today and in the future. *J Geod* 85:909–920. <https://doi.org/10.1007/s00190-0100427-x>
- Bilitza D, Altadill D, Zhang Y, Mertens C, Truhlik V, Richards P, McKinnell LA, Reinisch B (2014) The international reference ionosphere 2012-a model of international collaboration. *J Space Weather Space Clim* 4:A07. <https://doi.org/10.1051/swsc/20140404>
- Bilitza D, Altadill D, Truhlik V et al (2017) International Reference Ionosphere 2016: from ionospheric climate to real-time weather predictions. *Space Weather* 15(2):418–429
- Birch MJ, Hargreaves JK, Bailey GJ (2002) On the use of an effective ionospheric height in electron content measurement by GPS reception. *Radio Sci* 37(1):1. <https://doi.org/10.1029/2000rs002601>
- Brown S, Bilitza D, Yigit E (2017) Ionosonde-based indices for improved representation of solar cycle variation in the international reference ionosphere model. *J Atmos Solar-Terr Phys*. <https://doi.org/10.1016/j.jastp.2017.08.022>
- Brunini C, Camilion E, Azpilicueta F (2011) Simulation study of the influence of the ionospheric layer height in the thin layer ionospheric model. *J Geod* 85(9):637–645. <https://doi.org/10.1007/s00190-011-0470-2>
- Chen Y, Liu L, Wan W (2011) Does the $F_{10.7}$ index correctly describe solar EUV flux during the deep solar minimum of 2007–2009. *J Geophys Res Space Phys* 116:A04304. <https://doi.org/10.1029/2010JA016301>
- Cherniak I, Zakharenkova I (2016) NeQuick and IRI-Plas model performance on topside electron content representation: spaceborne GPS measurements. *Radio Sci* 51(6):752–766
- Cherniak I, Zakharenkova I, Redmon RJ (2015) Dynamics of the high-latitude ionospheric irregularities during the 17 March 2015 St. Patrick's Day storm: ground-based GPS measurements. *Space Weather* 13:585–597. <https://doi.org/10.1002/2015SW001237>
- Crowley G et al (2006) Global thermosphere-ionosphere response to onset of 20 November 2003 storm. *J Geophys Res* 111:A10S18. <https://doi.org/10.1029/2005ja011518>
- Danilov AD (2013) Ionospheric F-region response to geomagnetic disturbances. *Adv Space Res* 52(3):343–366. <https://doi.org/10.1016/j.asr.2013.04.019>

- Foster JC, Coster AJ, Erickson PJ et al (2005) Multiradar observations of the polar tongue of ionization. *J Geophys Res* 110:A09S31. <https://doi.org/10.1029/2004JA010928>
- Gulyaeva TL, Arikani F, Sezen U et al (2018) Eight proxy indices of solar activity for the international reference ionosphere and plasmasphere model. *J Atmos Solar Terr Phys* 172:122–128
- Habarulema JB, Ssessanga N (2017) Adapting a climatology model to improve estimation of ionosphere parameters and subsequent validation with radio occultation and ionosonde data. *Space Weather* 15(1):84–98
- Hernandez-Pajares M, Juan JM, Sanz J, Bilitza D (2002) Combining GPS measurements and IRI model values for space weather specification. *Adv Space Res* 29(6):949–958. [https://doi.org/10.1016/S0273-1177\(02\)00051-0](https://doi.org/10.1016/S0273-1177(02)00051-0)
- Huang X, Reinisch BW (1996) Vertical electron density profiles from digisonde ionograms: The average representative profile. *Ann Geofis XXXIX*(4):751–756
- Huang CS, Foster JC, Goncharenko LP, Erickson PJ, Rideout W, Coster AJ (2005) A strong positive phase of ionospheric storms observed by the Millstone Hill incoherent scatter radar and global GPS network. *J Geophys Res* 110:A06303. <https://doi.org/10.1029/2004JA010865>
- Klimenko MV, Klimenko VV, Zakharenkova IE, Cherniak IV (2015) The global morphology of the plasmaspheric electron content during Northern winter 2009 based on GPS/COSMIC observation and GSM TIP model results. *Adv Space Res* 55:2077–2085. <https://doi.org/10.1016/j.asr.2014.06.027>
- Komjathy A, Langley R (1996) Improvement of a global ionospheric model to provide ionospheric range error corrections for single-frequency GPS users. In: Proceedings of the 52nd annual meeting of the institute of navigation, Cambridge, MA, June 1996. pp 557–566
- Lanyi GE, Roth T (1988) A comparison of mapped and measured total ionospheric electron content using global positioning system and beacon satellite observations. *Radio Sci* 23(4):483–492
- Lei J et al (2007) Comparison of COSMIC ionospheric measurements with ground-based observations and model predictions: preliminary results. *J Geophys Res* 112:A07308. <https://doi.org/10.1029/2006JA012240>
- Li M, Yuan Y, Zhang B et al (2018) Determination of the optimized single-layer ionospheric height for electron content measurements over China. *J Geodesy* 92(2):169–183
- Liu R, Smith P, King J (1983) A new solar index which leads to improved foF2 predictions using the CCIR Atlas. *Telecommun J* 50:408–414
- Liu L, Yao Y, Kong J, Shan L (2018) Plasmaspheric electron content inferred from residuals between GNSS-Derived and TOPEX/JASON vertical TEC data. *Remote Sens* 10(4):621
- Mannucci AJ, Wilson BD, Yuan DN, Ho CH, Lindqwister UJ, Runge TF (1998) A global mapping technique for GPS-derived ionospheric total electron content measurements. *Radio Sci* 33(3):565–582. <https://doi.org/10.1029/97rs02707>
- Migoya-Oru  Y, Nava B, Radicella S, Alazo-Cuartas K (2015) GNSS derived TEC data ingestion into IRI 2012. *Adv Space Res* 55(8):1994–2002
- Nava B, Radicella SM, Leitinger R, Coisson P (2007) Use of total electron content data to analyze ionosphere electron density gradients. *Adv Space Res* 39(8):1292–1297. <https://doi.org/10.1016/j.asr.2007.01.04>
- Nava B, Coisson P, Radicella SM (2008) A new version of the NeQuick ionosphere electron density model. *J Atmos Solar Terr Phys* 70(15):1856–1862
- Nayak C, Tsai LC, Su SY, Galkin IA, Tan ATK, Nofri E, Jamjareegulgarn P (2016) Peculiar features of the low-latitude and midlatitude ionospheric response to the St. Patrick’s Day geomagnetic storm of 17 March 2015. *J Geophys Res Space Phys* 121:7941–7960. <https://doi.org/10.1002/2016JA022489>
- Nayir H, Arikani F, Arikani O, Erol CB (2007) Total electron content estimation with Reg-Est. *J Geophys Res: Space Phys.* <https://doi.org/10.1029/2007ja012459>
- Okoh D, McKinnell LA, Cilliers P et al (2013) Using GPS-TEC data to calibrate VTEC computed with the IRI model over Nigeria. *Adv Space Res* 52(10):1791–1797
- Pedatella NM, Yue X, Schreiner WS (2015) Comparison between GPS radio occultation electron densities and in situ satellite observations. *Radio Sci* 34:949–966. <https://doi.org/10.1002/2015RS005677>
- Pignalberi A, Pezzopane M, Rizzi R, Galkin I (2018) Effective solar indices for ionospheric modeling: a review and a proposal for a real-time regional IRI. *Surv Geophys* 39(1):125–167
- Sezen U, Arikani F, Arikani O, Ugurlu O, Sadeghimorad A (2013) Online, automatic, near real-time estimation of GPS-TEC: iONOLAB-TEC. *Space Weather* 11(5):297–305. <https://doi.org/10.1002/swe.20054>
- Tapping KF (2013) The 10.7 cm solar radio flux (F10.7). *Space Weather* 11(7):394–406
- Yao Y, Liu L, Kong J, Zhai C (2016) Analysis of the global ionospheric disturbances of the March 2015 great storm. *J Geophys Res: Space Phys* 121(12):12–157
- Yizengaw E, Moldwin MB, Galvan D et al (2008) Global plasmaspheric TEC and its relative contribution to GPS TEC. *J Atmos Solar Terr Phys* 70(11–12):1541–1548
- Yue X, Schreiner WS, Rocken C, Kuo YH (2011) Evaluation of the orbit altitude electron density estimation and its effect on the Abel inversion from radio occultation measurements. *Radio Sci* 46:RS1013. <https://doi.org/10.1029/2010rs004514>
- Zou S, Ridley AJ, Moldwin MB et al (2013) Multi-instrument observations of SED during 24–25 October 2011 storm: implications for SED formation processes. *J Geophys Res: Space Phys* 118(12):7798–7809